Antireflective GaN nanoridge texturing by metal-assisted chemical etching via thermally dewetted Pt catalyst network for highly responsive ultraviolet photodiodes

Yikai Liao,[1] You Jin Kim,[1] Junyu Lai,[2] Jung-Hun Seo,[2] and Munho Kim[1]*

[1]School of Electrical and Electronic Engineering, Nanyang Technological University, 50 Nanyang Avenue, 639798 Singapore, Singapore
[2]Department of Materials Design and Innovation, University at Buffalo, The State University of New York, Buffalo, NY 14260 USA

Email: munho.kim@ntu.edu.sg

Keywords: antireflection, gallium nitride, photodiode, ultraviolet, metal-assisted chemical etching

Abstract

Antireflective surface texturing is a feasible way to boost the light absorption of photosensitive materials and devices. As a plasma-free etching method, metal-assisted chemical etching (MacEtch) has been employed for fabricating GaN antireflective surface texturing. However, the poor etching efficiency of typical MacEtch hinders the demonstration of highly responsive photodetectors on undoped GaN wafer. In addition, GaN MacEtch requires metal mask patterning by lithography, which leads to a huge processing complexity when the dimension of GaN antireflective nanostructure scales down to the sub-micron range. In this work, we have developed a facile texturing method of forming a GaN nanoridge surface on undoped GaN thin film by lithography-free sub-micron mask patterning process via a thermal dewetting of platinum. The nanoridge surface texturing effectively reduces the surface reflection in ultraviolet (UV) regime, which can be translated to a six-fold enhancement in responsivity (i.e., 115 A/W) of photodiode at 365 nm. The results demonstrated in this work show that MacEtch can offer a viable route for enhanced UV light-matter interaction and surface engineering in GaN UV optoelectronic devices.

1. Introduction

In recent years, a demand for highly responsive ultraviolet (UV) photosensing has been growing due to the requirement for increased photo-sensitivity in various fields such as monitoring of environmental and biological analysis, optical communication, and astronomy studies[1]. Considering the detection wavelength range in UV region, numerous wide band gap semiconductors such as gallium nitride (GaN), zinc oxide (ZnO) and gallium oxide (Ga_2O_3) have been studied intensively[2]. Among them, GaN is regarded as one of the best candidates for UV photodetection due to its direct band gap characteristic with suitable band gap energy, high electron mobility and commercial availability of high quality crystal substrates as well as epitaxial thin films[3].

Surface antireflective (AR) treatment has been proven effective in boosting the light absorption within the materials[4, 5] as a widely employed approach to enhance the light harvesting capability of photosensing devices. Compared with AR coating of layer stacks which requires a precise control of the parameters such as refractive index and thickness, AR surface texturing via nanostructures by top-down etching method exhibits merits such as omnidirectional, broadband AR characteristics and facile fabrication process[4]. For GaN, various nanostructures such as nanopillars[6-8], nanopyramids[9], nanodomes[10, 11] and porous GaN[12, 13] have been fabricated by either dry (plasma) etching[6, 7, 14, 15] or anisotropic wet (chemical) etching[8, 12, 13, 16]. The former method typically involves lithography-patterned[15] or thermally dewetted metal hard mask[6, 7, 11, 14] for subsequent dry etching of GaN. However, it is notable that dry etching of GaN introduces undesirable damages and defects[17], resulting in large dark current in photodetectors[18] and leakage current in power devices[19, 20]. On the contrary, such plasma-induced surface damage can be avoided by wet etching. Therefore, anisotropic wet chemical etching is employed to produce GaN antireflective structures. Doped GaN[12, 21] are typically utilized, due to a low etching efficiency of undoped GaN[22, 23], forming porous structures. However, previous literatures show that Schottky barrier diodes based on doped GaN exhibit higher leakage current and lower UV responsivity compared to those made on undoped GaN thin films due to a lower concentration of Ga vacancies in undoped GaN epi-layers[24, 25]. In addition, undoped GaN exhibits higher electron mobility than doped one[26], which exhibits better application potential in high speed device. Therefore, undoped GaN antireflective structures via anisotropic wet etching offer an appealing option for high performance UV photodetectors.

However, the reports on wet etching of undoped GaN for device level applications have not yet been well studied. Although some groups have demonstrated a porous surface on undoped GaN, its electrical and optical properties were not studied[27-29]. There have been attempts to employ porous surface texturing on undoped GaN in UV photodetection, but they failed to achieve enhanced responsivity. For example, Guo et. al[30] utilized porous undoped GaN to detect 325 nm UV light. However, responsivity was deteriorated after porosification treatment, probably due to the increased surface states from high surface-to-volume ratio of the porous structure. Therefore, it is worthwhile to carry out a comprehensive study of an anisotropic wet etching method on undoped GaN to fabricate antireflective GaN for highly responsive UV photodetectors.

Among various anisotropic wet etching methods, metal-assisted chemical etching (*i.e.* MacEtch, also named as electroless chemical etching or photoenhanced wet etching for GaN) is more preferred since it is a simple alternative to photoelectrochemical etching which requires external electrical contact to sample[31]. Since MacEtch of GaN is catalyzed by noble metal catalyst (typically platinum (Pt)[30, 32]), a Pt catalyst patterning process is required on the GaN surface[32-34]. Bardwell has shown that the etching rate variation of GaN occurs due to the in-plane distance to Pt catalyst[31].

Therefore, it is important to keep the distance small between Pt-pattern areas to realize uniform etching across the sample surface. In addition, nanostructures with dimension and spacing comparable and even smaller than incident wavelength are desirable to realize efficient light-matter interactions[4, 5]. Therefore, sub-micron size Pt-patterned areas are required for GaN MacEtch which can be realized by electron beam lithography (EBL)[35] or nanosphere lithography[36]. However, these processes are either resource-consuming or requiring complex chemical patterning process. As a result, a facile and cost-effective sub-micron Pt catalyst patterning process is well desired to form densely distributed antireflective GaN nanostructures.

Here, inspired by the thermally driven dewetting characteristic[37, 38] and catalyst function of Pt, we put forward a sub-micron Pt catalyst network for GaN MacEtch to fabricate the textured GaN surface with densely packed undoped GaN nanoridge structures. This high-quality textured GaN surface was then systematically characterized to reveal its structural, optical and electrical properties, as well as UV photodetecting performance of photodiodes. Compared with photodiodes made on planar GaN surfaces, the GaN nanoridge photodiodes are capable of realizing a six-fold increase in responsivity. Our result shows that the plasma-free and lithography-free MacEtch can be a viable and cost-effective technique to form GaN AR nanostructures that enable a translation of the enhanced UV optical properties into optoelectrical performance at the device level.

2. Experimental Section

The process starts with the GaN wafer that has a 4.5 μm thick unintentionally doped n-type GaN epilayers on sapphire (c-Al_2O_3) by metal organic chemical vapor deposition (MOCVD) from Biotain Crystal. Samples were cleaned by sonicated acetone, isopropanol alcohol (IPA) and deionized water subsequently for 5 min each, then immersed in the diluted hydrochloric acid (HCl, 10%) to remove native oxide. Samples were then loaded into electron-beam (e-beam) evaporator (Edwards Auto306) to deposit 10 nm Pt thin film with a deposition rate of 0.1 Å/s. Thermal dewetting of evaporated Pt thin film was carried out at 900 ℃ in nitrogen atmosphere (N_2) by rapid thermal annealing system (RTA, AS-ONE AnnealSys).

GaN MacEtch was performed in a mixed etchant of potassium persulfate ($K_2S_2O_8$, 40.7 mM) and hydrofluoric acid (HF, 14 M). Prior to etching, solution was stirred with a magnetic stir bar to ensure a complete dissolution of $K_2S_2O_8$ in etchant. Then, GaN samples with dewetting-patterned Pt mask were immersed in the etchant under the illumination of a 254 nm ultraviolet (UV) lamp with a light power of 8 W at room temperature. Distance between UV lamp and GaN samples was fixed at ~3 cm. Etching was carried out at static environment without stirring etchant. After GaN MacEtch, GaN samples were cleaned with DI water and blown dry with N_2 gun. Residue of Pt catalyst was removed by aqua regia treatment (50 ℃, 2 min) in order to minimize its influence on etched GaN surface. Then, GaN metal-semiconductor-metal (MSM) photodiodes were fabricated by depositing Ti/Au (20/80 nm) interdigital electrodes with a finger width and spacing of 4 μm and 4 μm respectively. The devices were fabricated on both nanoridge (etched) and planar (unetched) GaN surfaces for comparison.

Field emission scanning electron microscope (FESEM, Sirion, FEI Netherlands) was used for surface morphology characterization. Hall effect measurement (HS-65-AEM) was carried out to characterize the electrical properties using soldering indium electrode for good ohmic contact with low contact resistance. Surface chemical composition was examined by X-ray photoelectron spectroscope (XPS, Kratos AXIS Supra). Photoluminescence (PL) spectrum was measured by

RPM2000 at room-temperature with a He-Cd 325 nm laser source. Raman spectra measurement was carried out under the backscattering condition using a UHT S300&WITEC Raman spectroscopy with a 532 nm laser focusing on a 1 μm diameter spot by using a 100× objective lens. Optical reflectance spectra were measured by UV–visible spectrometer (Shimadzu UV-2450) using an integrating sphere. Lumerical finite difference-time-domain (FDTD) was used for optical simulation with the refractive index (n) and extinction coefficient (k) of wurtzite GaN extracted from ref. [39][39]. A plane-wave light source was adopted for normal incident illumination with a perfectly matched layer (PML) utilized in vertical ends and the reflectance monitor located at the backside of the light source. Electrical characteristics of photodiodes were measured using a Keithley 4200 SCS semiconductor analyzer in the dark box. For device measurement under illumination, UV– visible light was illuminated directly from Horiba 150 W Xe tunable light source using a Formfactor light wave probe.

3. Results and Discussion

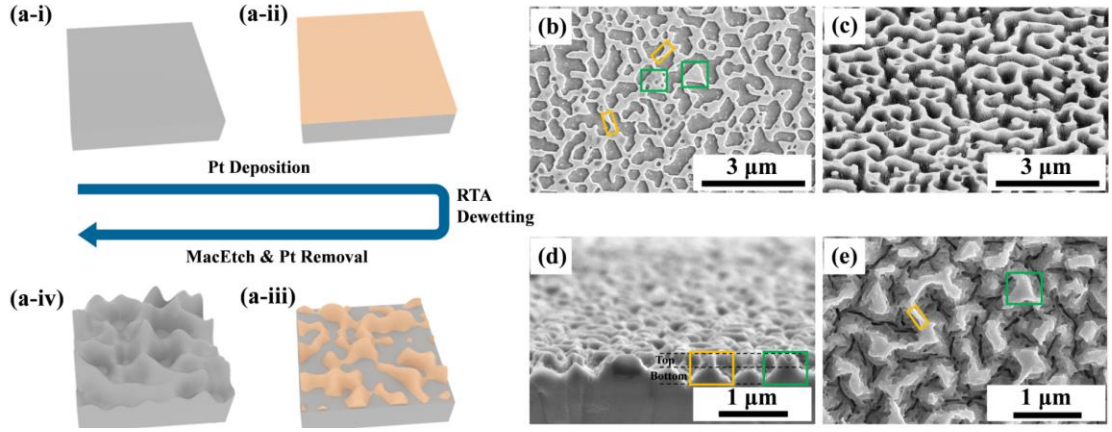

Figure 1. (a) Fabrication process of GaN nanoridge structures. (b) Top SEM image of 180 s RTA dewetted Pt network on GaN. (c) Tilted SEM image of GaN nanoridge structures before Pt removal. (d) Cross-sectional and (e) top-view SEM images of GaN nanoridge structure after Pt removal.

Figure 1a shows the fabrication process of GaN nanoridge structures. After GaN sample cleaning (Figure 1a-i), a 10 nm Pt thin film was evaporated onto GaN samples (Figure 1a-ii), with top-view SEM image shown in Figure S1. Dewetting of Pt thin film was carried out by RTA at 900 ℃ for 180 s in N_2 atmosphere, changing Pt from continuous thin film to network structure as indicated by Figure 1a-iii and Figure 1b. Pt network mainly consists of larger clusters (in-plane dimension larger than 250 nm, green box in Figure 1b) and thin interconnects (in-plane dimension ~100 nm, orange box in Figure 1b). GaN samples covered with the dewetted Pt network then underwent MacEtch process under UV illumination for 15 min. As shown in Figure 1c, GaN was etched at areas not covered by the Pt catalyst, indicating the inverse nature of UV-assisted MacEtch of wide band gap semiconductors[8, 40]. After removal of the Pt residues, the formation of GaN nanoridge structures with 500 nm height was completed as shown in cross-sectional (Figure 1d) and top SEM (Figure 1e) images. It can be clearly seen that the nanoridge has a sharp tip (indicated by "Top" in Figure 1d) and obtuse base (in-plane dimension ~ 500 nm, indicated by "Bottom" in Figure 1d). It indicates that MacEtch of GaN was anisotropic in the early stage of the etching, creating vertical sidewalls

while at a later stage, the vertical direction etching became slower, thus the overall etching tended to be more isotropic. MacEtch of GaN is mainly governed by the following process[31, 41].

Photons were absorbed by GaN, generating electrons (e^-) and holes (p^+) within the GaN:

$$GaN + photon \rightarrow GaN + e^- + p^+ \quad (1)$$

Under UV light with wavelength smaller than 310 nm, $S_2O_8^{2-}$ absorbed photons, generating sulfate ion radical ($SO_4^{-\bullet}$) which is a strong oxidizing agent catalyzed by Pt:

$$S_2O_8^{2-} + photons \rightarrow 2SO_4^{-\bullet} \quad (2)$$

Therefore, photogenerated electrons could be consumed by $SO_4^{-\bullet}$:

$$SO_4^{-\bullet} + e^- \rightarrow SO_4^{2-} \quad (3)$$

While photogenerated holes participated in oxidizing GaN:

$$GaN + 3\,p^+ \rightarrow Ga^{3+} + 1/2\,N_2 \quad (4)$$

Ga^{3+} is generally considered in the form of Ga_2O_3[41, 42], which can be further dissolved in the same etching environment[40, 43].

Sulfate ion radical formation is a crucial step for the following GaN etching, which is catalyzed by Pt. Therefore, the anisotropic etching characteristic in the early stage of the MacEtch is likely from its closer distance to the surface with Pt catalysts. It results in the formation of sharp tips at the top of nanoridge, while at the later stage of the etching, such effect got weaken, resulting in less anisotropic etching (*i.e.*, an obtuse base of the nanoridge). Similar dual sidewall morphology has been observed in inverse-MacEtch (*i*-MacEtch) of Ge in which Ge pyramid has sharp top sidewalls with rounded base[44]. In addition, thermal dewetting formed two kinds of Pt mask morphologies (larger cluster and thin interconnects indicated by orange and green boxes in Figure 1b respectively). It leads to the formation of narrow (~100 nm top width) and wide tips (~300 nm top width) at the top region (~200 nm height) of nanoridges as indicated by orange and green boxes respectively in Figure 1d and 1e after MacEtch. Figure S2 illustrates the combination of Pt dewetting and MacEtch is able to realize uniform fabrication of GaN nanoridge surface texturing across the sample with size over 1cm*1cm.

To study the effect of the in-plane Pt morphologies on the resultant nanostructures, we extended the RTA dewetting time from 180 s (Figure 1) to a broader range from 60 to 240 s (Figure S3). Other conditions remained unchanged. Pt dewetting of 60 s resulted in sparse and small voids in the Pt layer. Prolonging dewetting time enlarged the voids and narrowed down the Pt-covered area. A similar evolution of Pt nanostructure has also been observed in Kunwar's work, in which metal adatoms can agglomerate more compactly with a longer annealing time[45]. Since the etching process occurred at the areas not covered by Pt, different morphologies of Pt catalyst led to different morphologies of GaN nanostructures as shown in Figure S3, in which MacEtch via 60 and 120 s dewetted Pt mask led to the small, dense and isolated GaN hillocks, while 180 and 240 s resulted in largely connected nanoridge structure. Figure S4a shows the dependence of etching depth (nanostructure height) on RTA dewetting time corresponding to SEM images in Figure S3. GaN nanostructure formed by MacEtch via 60 s dewetted Pt mask has the lowest height of ~ 250 nm. It should be due to the limited access of GaN to etchant since most GaN surface areas were covered by Pt. Enlargement of voids in the Pt mask led to improved access of etchant to GaN, therefore larger nanostructure depth can be realized. A maximum nanoridge height of 500 nm was achieved via 180 s dewetted Pt mask. Further prolonging the dewetting time to 240 s led to decreasing etching depth, likely due to the further narrowing down of the Pt covered area. Photogenerated electrons in GaN moved from GaN through the GaN/Pt interface to Pt, then got consumed, leaving

photogenerated holes behind in GaN which participated in the subsequent etching. Thus, a smaller interface area might slow down the transport of electrons, which led to a slower etching rate. As a result, GaN nanostructure has a height of ~410 nm via 240 s dewetted Pt mask. Another possible reason is that 240 s dewetted narrow Pt mask is more easily influenced by the lateral etching of GaN and more likely delaminated from GaN surface. Therefore, etching tended to be slower if the bonding between Pt and GaN became weaker by undercut. Figure S4b shows the dependence of nanoridge height (etching depth) on etching time using 180 s dewetted GaN network (Figure 1b). Etching tended to slow down at the later stage of the MacEtch, which is also likely from the influence of the undercut.

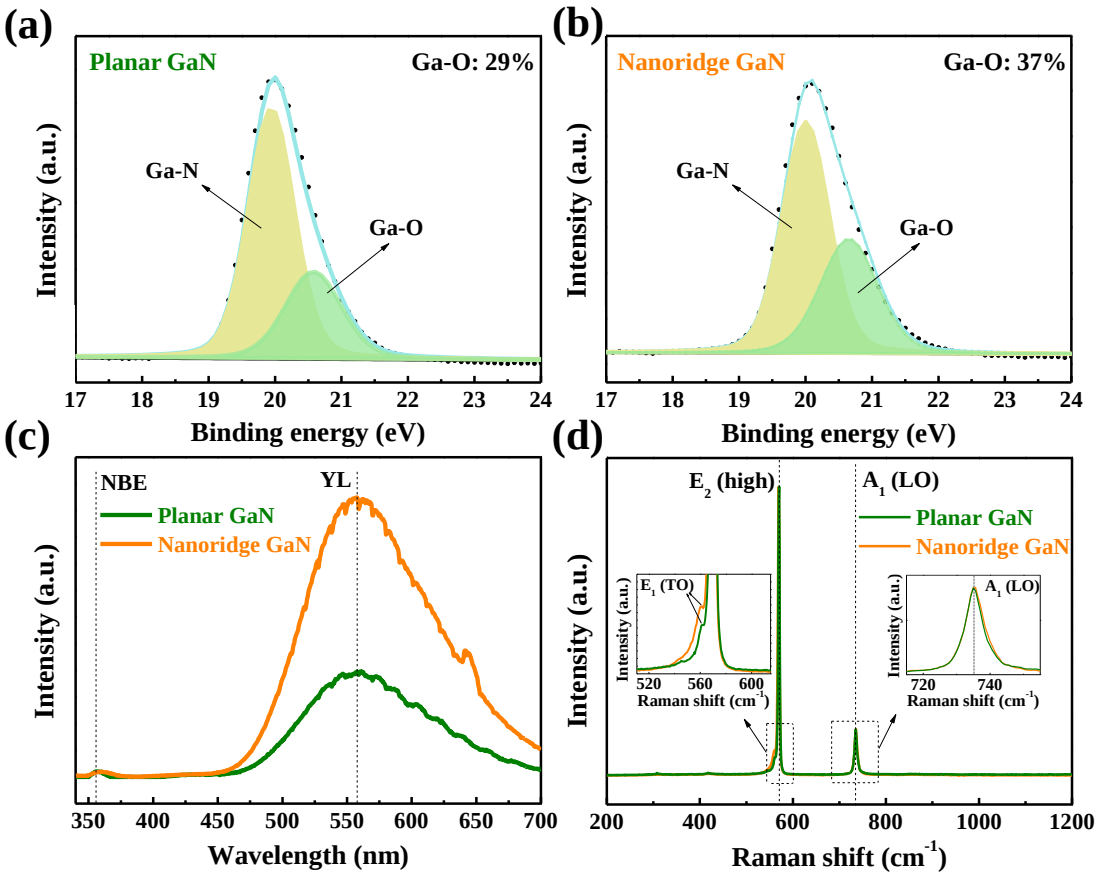

Figure 2. Ga 3d XPS spectra of (a) planar GaN and (b) nanoridge GaN surfaces. Dotted lines indicate the raw data while solid lines indicate the peak fitting result. (c) Room-temperature PL spectra and (d) room-temperature Raman spectra of planar and nanoridge GaN surfaces. Insets in Figure 2d show the amplified spectra in peak regions indicated by black arrows.

XPS measurement was carried out to characterize the change of surface chemical composition before and after MacEtch via 180 s dewetted Pt network. Figure 2a and b show the Ga 3d spectra of planar and nanoridge GaN, respectively, with a binding energy corrected by C 1s peak. Two peaks can be distinguished using peak fitting and assigned to Ga-N and Ga-O composition[46]. Compared with planar GaN, nanoridge GaN surface has a higher Ga-O composition ratio, which is from the oxidation of GaN to Ga_2O_3 indicated by the equation (4). Due to the difference in surface composition, the Ga 3d peak position of nanoridge GaN shows a clear shift from planar GaN as shown in Figure S5. Figure 2c shows the room-temperature PL spectra of planar and nanoridge GaN,

with the normalized peak at 360 nm. Two major PL peaks locating at 360 nm and 560 nm can be assigned to near-band-edge emission (NBE) and yellow luminescence (YL), respectively[8]. The NBE peak shows much lower intensity compared with YL peak, which is likely from the low carrier concentration in undoped GaN[28]. Compared with planar GaN, nanoridge GaN surface shows a much higher YL peak intensity. YL in undoped GaN is widely regarded to be from the complexes of gallium vacancies and oxygen substituting on the nitrogen site (V_{Ga}-O_N complexes)[47]. Therefore, such complexes were promoted by the incorporation of oxygen into GaN as indicated by XPS measurement during MacEtch, resulting in a stronger YL peak. It is notable that the correlation of YL in GaN with the surface oxidation layer has been reported by Shalish *et. al*[48]. Figure 2d shows the room-temperature Raman spectra of planar and nanoridge GaN surfaces, with Raman intensity normalized to peak locating at 569 cm^{-1}. Two major Raman peaks located at 569 cm^{-1} and 735 cm^{-1} can be assigned to E_2 (high) and A_1 (LO) of wurtzite GaN, respectively[49]. As shown in the left inset in Figure 2d, E_1 (TO) peak locating at the shoulder of E_1 (high) shows enhanced intensity after MacEtch, which is due to the exposure of other crystal planes besides (0001) GaN on the surface[50]. As shown in the right inset in Figure 2d, A_1 (LO) peak shows a slightly broadened characteristic with a peak position shifted to higher wavenumber after MacEtch. It is notable that such changes in position and broadness of A_1 (LO) peak indicate an increase in carrier concentration within GaN[49].

Table 1. Sheet resistivity, hall mobility and carrier concentration of planar and nanoridge GaN from Hall measurement.

Materials	Sheet resistivity (Ω-cm)	Hall mobility ($cm^2/V•s$)	Carrier concentration ($1/cm^3$)
Planar GaN	0.4219	395.1173	3.75×10^{16}
Nanoridge GaN	0.1645	309.9696	1.23×10^{17}

In order to confirm the possible change of electrical property of GaN before and after MacEtch, we performed room-temperature Hall effect measurement using the Van der Pauw method[51]. Table 1 shows the key extracted parameters. After MacEtch, carrier concentration in GaN increased from $3.75 \times 10^{16}/cm^3$ to $1.23 \times 10^{17}/cm^3$. Since oxygen substituting on the nitrogen site is a shallow donor in GaN[52], the incorporation of oxygen in GaN during MacEtch led to the enhancement of n-type doping, thus increasing carrier concentration. A similar change in carrier concentration has been observed in GaN surface that was processed by the remote plasma oxidation[53]. Therefore, lower sheet resistivity is from the higher carrier concentration after MacEtch, while lower hall mobility might be from enhanced scattering by means of impurity scattering and electron-electron scattering[54]. Since YL peak in GaN PL is related with electron transition from conduction band or from a shallow donor to a deep acceptor[47], the increased carrier concentration after MacEtch may also contribute to the increased YL peak intensity (Figure 2c).

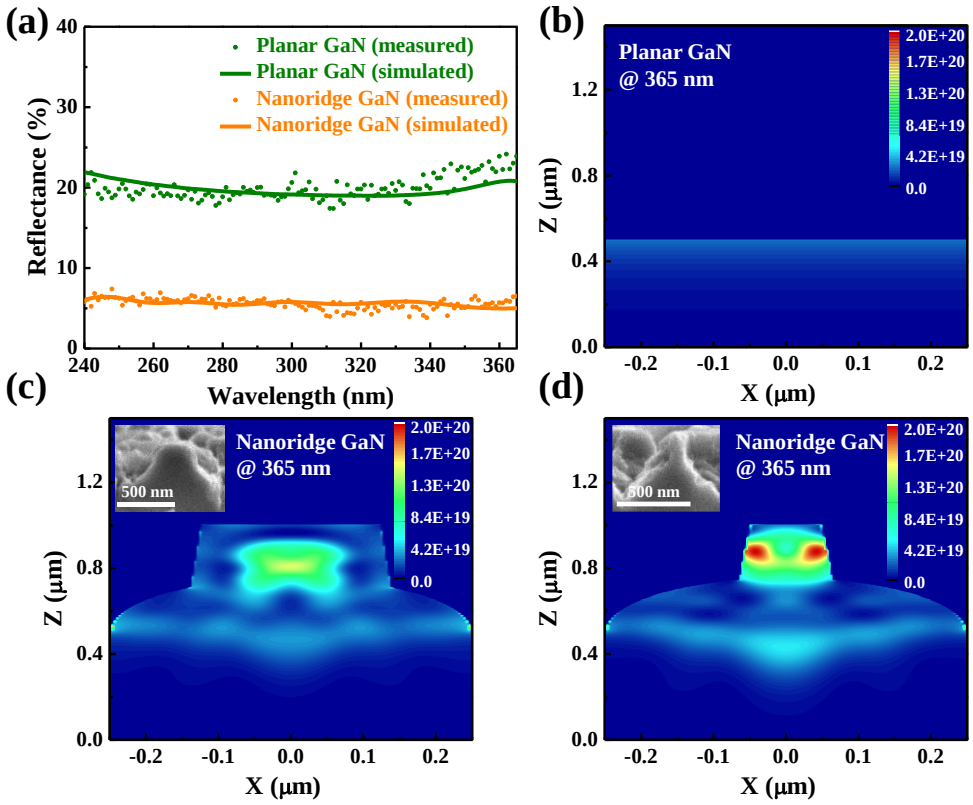

Figure 3. (a) Measured (dotted) and FDTD simulated (solid) UV reflectance spectra of planar (green) and nanoridge (orange) GaN surfaces. Cross-sections of power absorption of (b) planar GaN, (c) nanoridge GaN with wide tip and (d) nanoridge GaN with narrow tip under 365 nm illumination. Scale bars in (b), (c) and (d) are aligned. Inset SEM images in (c) and (d) indicate two actual tip morphologies of nanoridge structures. Note that the nanoridge structure was formed by MacEtch via 180 s dewetted Pt network. FDTD simulated reflectance spectrum (orange, solid line) in Figure 3a was obtained from the average of spectra modeled by Figure 3c and 3d.

To study AR performance of the nanoridge GaN, UV reflectance spectra of the GaN nanoridge structure were measured by UV-visible spectrometer (Figure 3a). FDTD simulation results were obtained with models built based on the actual dimensions of the GaN nanoridges shown in SEM image of Figure 1d. Reflectance of the GaN nanoridge structure was measured to be ~5 % in a wavelength range of 240 to 365 nm, while planar GaN had an average reflectance over 20 % in the same UV range. It indicates a clear AR capability of the GaN nanoridges in UV range. The reduced reflectance is attributed to the multiple internal reflection, leading to longer light paths within the GaN nanostructures[4, 5]. It is so because the dimensional parameters of the GaN nanoridge structures such as height and periodicity are comparable with the UV wavelength used in this study[55].
Furthermore, it is important to have a better insight into how enhanced AR performance is realized by the nanoridge structure. Thus, we performed FDTD simulation to reveal electric field distribution of GaN nanoridge structure when illuminated by 365 nm plane wave light (Figure S6). Two tip morphologies formed at the top of nanoridges were built in FDTD simulation. FDTD simulated reflectance spectra of both nanoridge models with different tip dimensions (Figure 3c and 3d) were given in Figure S7. For the planar GaN, the out-of-plan periodic electric field is due to the

constructive and destructive interference of the incident and reflective light[56], with electric field inside GaN remaining low intensity (blue/cyan color). For the nanoridge GaN, enhanced electric field intensity is observed within the nanoridge structure, especially in the tip regions (green/yellow color). It indicates the strong coupling of incident light within GaN nanoridge[57]. Figure 3b, c and d show the cross-sections of power absorption of planar and nanoridge GaN under 365 nm UV irradiation. Inset SEM images in Figure 3c and 3d show the corresponding morphologies of the nanoridge. Owing to the strong coupling of UV light and GaN nanoridge, GaN nanoridge structure achieves a much stronger absorption intensity compared to that of the planar GaN at 365 nm. Since GaN barely transmits the UV light with wavelengths shorter than 365 nm[58], the reduced reflectance directly leads to the enhanced light absorption. Reflectance spectra of GaN nanostructures by MacEtch via dewetting times of 60, 120, and 240 s (Figure S3) are shown in Figure S8a. Although the difference in reduced reflectance is not significant, the nanostructure by MacEtch via 180 s dewetted Pt network shows the lowest reflectance in the UV wavelength range, probably due to its largest nanoridge height as shown in Figure S4a. In addition, since different etching time leads to different heights of nanostructures (Figure S4b), their corresponding reflectance spectra were shown in Figure S8b. GaN nanoridge structure by 15 min MacEtch shows the lowest reflectance due to its largest height. Therefore, since GaN nanoridge structure by 15 min MacEtch using 180 s dewetted Pt catalyst network has the lowest reflectance, we focus on this structure to study how optimal optical properties are translated into device performance.

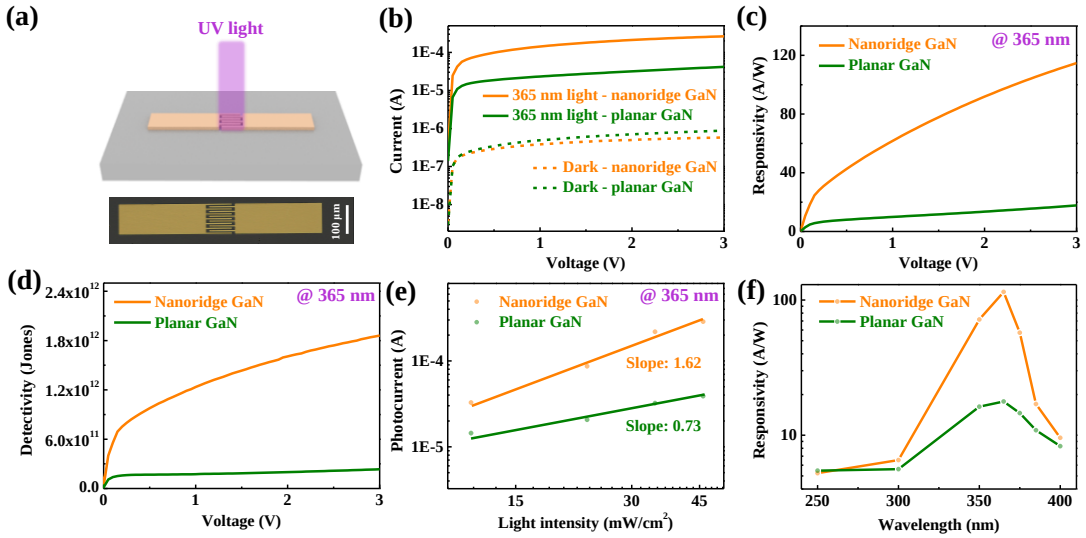

Figure 4. (a) Schematic illustration of GaN MSM photodiode with top-view optical microscope image shown at the bottom part. (b) Dark currents (dashed lines) and photocurrents (solid lines) of GaN photodiodes based on the planar (green) and nanoridge (orange) surfaces under 365 nm UV illumination with the light intensity fixed at 46 mW/cm^2. (c) Responsivity and (d) detectivity of photodiodes under 365 nm UV light. (e) Photocurrent of photodiodes as a function of incident light intensity under 365 nm UV illumination in log scale with 3 V bias. (f) Spectral responsivity of photodiodes in the wavelength range of 250 to 400 nm.

Metal-semiconductor-metal (MSM) UV photodiodes were fabricated on both planar and nanoridge GaN surfaces as shown in Figure 4a. Figure 4b shows the dark currents and photocurrents under

365 nm UV illumination, respectively. Photodiode based on nanoridge GaN shows a slightly lower dark current compared with planar GaN, which we attribute it to the change of contact interface between metal electrode and etched GaN. We have also fabricated Schottky diodes on both surfaces to study the effect of the contact interface on the device performance (Figure S9a). By using two methods shown in Figure S9, the extracted Schottky barrier height between Ti/Au and nanoridge GaN shows 0.04 eV higher than that of planar GaN. We attribute the lower dark current and the higher Schottky barrier height to the surface oxidation layer (Figure 2a and b). A similar effect of the oxidation layer on n-GaN diodes has been reported, in which an additional barrier from surface oxidation layer suppressed electron tunneling through field emission and thermionic field emission, leading to smaller reverse current of Schottky diodes[59]. Contrary to dark current, nanoridge GaN photodiode shows a much higher photocurrent under 365 nm illumination than that of planar GaN photodiode. It indicates that the enhanced light absorption by the nanoridge structure (Figure 3) has been effectively translated into the enhanced responsivity.

We have extracted key parameters (e.g., responsivity (R), detectivity (D^*) and external quantum efficiency (EQE)) of the photodiodes based on the current-voltage characteristics of photodiodes in Figure 4b using the following equations[56]:

$$R = \frac{I_{photo} - I_{dark}}{P_\lambda S} \quad (5)$$

$$D^* = \frac{\sqrt{S}R}{\sqrt{2qI_{dark}}} \quad (6)$$

$$EQE = \frac{Rhc}{\lambda q} \quad (7)$$

where I_{photo} and I_{dark} are photocurrent and dark current respectively, p_λ is the incident light intensity (46 mW/cm^2) and S is the effective illumination area on the photodiode. q, h, c and λ are elementary charge, Planck constant, speed of light and wavelength of incident light (365 nm), respectively. The calculated R, D^* and EQE are shown in Figure 4c, 4d and S10, respectively. Distinctly enhanced R, D^* and EQE were achieved with nanoridge GaN surface. Especially, nanoridge GaN photodiode reaches a R value of 115 A/W, D^* of 1.86×10^{12} Jones and EQE of 39072% under a bias of 3 V, while those of planar GaN photodiode are 18 A/W, 2.34×10^{11} Jones and 5967%, respectively. Therefore, it leads to an overall 6-8 times enhancement in sensing capability by using the GaN nanoridge structure. Figure 4e shows the incident power intensity dependent photocurrents fitted by the power law as the following[56], with measured I-V plots shown in Figure S11:

$$I_{photo} = CP_\lambda^\theta \quad (8)$$

where C is a constant and θ is the empirical coefficient. By a linear fitting as shown in Figure 4e, θ is extracted to be 1.62 and 0.73 for photodiodes made on nanoridge and planar GaN, respectively. This indicates the photocurrent gain mechanism in GaN nanoridge photodiode[56, 60], which is due to the barrier height lowering by photogenerated holes trapped at metal-semiconductor interface[61, 62]. Table 2 shows the benchmarking of our device with other reported GaN based UV photodiodes. Despite working at relatively low bias and the simple device structure, our device has comparable and even higher responsivity and detectivity than those of other reports. We have also fabricated 10 photodiodes across the 1cm*1cm nanoridge GaN sample surface indicated in Figure S2. The photoresponse of devices (I_{photo}-I_{dark}) was shown in Figure S12. Despite covering centimeter-scale sample area, the PDs fabricated in different regions can show good consistency in photoresponse

performance.

Table 2. Comparison of photodetection performance among nanoridge GaN MSM photodiode (PD) and previously reported GaN-based PDs.

Photodetector type	Working bias (V)	λ (nm)	R (A/W)	D^* (Jones)	Rise time (s)	Decay time (s)	Reference
Nanoridge GaN MSM PD	3	365	115	1.86×10^{12}	2.1	3.8	This work
Planar GaN MSM PD	3	365	18	2.34×10^{11}	0.8	18.0	This work
GaN nanocolumn MSM PD	2	325	24	1.15×10^{11}	/	/	Ramesh, et. al[63]
Porous GaN/MoO_3 junction PD	3	370	0.187	4.34×10^{12}	/	/	Guo, et. al[64]
GaN p-i-n-i-p PD	5	358	11.7	N/A	0.029	0.038	Jiang, *et.al*[65]
Graphene/GaN Schottky PD	-10	325	5.83	1×10^{11}	0.003	0.005	Tian, *et. al*[66]
MoS_2/GaN junction PD	5	365	27.1	1.7×10^{10}	0.3	3.9	Zhang, *et. al*[67]

Apart from photoresponse to 365 nm UV light as discussed above, spectral photoresponse from 250 to 400 nm has also been measured (Figure 4f). Figure S13 shows the current-voltage curves measured under different wavelengths. The GaN nanoridge structure is able to effectively enhance the responsivity from 300-400 nm wavelength range, nonetheless such enhancement tends to degrade in the solar-blind region. We attribute the degradation in the short wavelength to the shallow absorption length of UV light in GaN. Figure S14 shows the cross-sections of power absorption of 250 nm UV light in planar and nanoridge GaN. The light absorption at 250 nm UV irradiation is limited to the top surface, causing weaker responsivity via local recombination of photogenerated carriers as well as surface recombination by surface states[56]. The slightly lower responsivity of nanoridge GaN photodiode at 250 nm than the planar one is also an indicator of surface recombination since MacEtch has introduced certain surface states as suggested by PL results.

In addition to the responsivity study, time-resolved response of the photodiodes to UV light (365 nm) are also provided in Figure S15. By using the bi-exponential fitting, two time constants (τ_1 and τ_2) can be extracted, corresponding to the fast- and slow-response component respectively in each rise/decay period of photodiode current. Typically, the fast-response component (τ_1) is an indicator of rapid change in carrier concentration once light is turned on/off while the slow-response component (τ_2) indicates carrier trapping/detrapping process governed by defects[68]. Therefore, higher τ_1 values of nanoridge GaN photodiode than planar one is due to the enhanced photocurrent gain of the device[69]. The τ_2 values of nanoridge GaN photodiode are distinctly larger than planar GaN, indicating the stronger influence of defects to carrier transport in nanoridge GaN, which is also consistent with the change of YL peak in PL analysis before and after MacEtch. In addition, the rise/decay time (defined as time required to increase current from 0 to 1-1/e of the maximum photocurrent and decrease maximum photocurrent to its 1/e value[70]) are given in Table 2. Despite the relatively slow response time compared with other GaN devices reported, our highly responsive

GaN UV PD via facile fabrication process still exhibits advantages when responsivity and detectivity are primary concerns.

4. Conclusions

In summary, we have demonstrated the fabrication of GaN UV photodiodes with highly enhanced responsivity by nanoridge surface texturing via MacEtch with a thermally dewetted Pt network. Dimension of nanoridge structure is comparable with wavelength of incident light, therefore the nanoridge surface texturing is capable of significantly reducing the UV reflection to 5%, which can be directly translated to enhanced UV light absorption within GaN. Surface oxidation layer on the textured surface formed during MacEtch is able to suppress the dark current of photodiode. Together with the significantly enhanced photocurrent from enhanced light absorption, the GaN UV photodiode fabricated on nanoridge surface exhibits high responsivity of 115 A/W at 365 nm, compared with 18 A/W on the planar surface. This result suggests that it is feasible to realize highly responsive GaN UV photodetector by low-cost fabrication process on commercially available GaN wafers, which sheds light on UV sensing industry.

Acknowledgment

This work was supported by the A*STAR, Singapore, Advanced Manufacturing and Engineering (AME) Young Individual Research Grant (YIRG) and IRG under the Project A2084c0066 and M21K2c0107, respectively, and Ministry of Education, Singapore, under the Grant ACRF Tier 2 grant (T2EP50120-0001). The authors acknowledge the support of the Nanyang NanoFabrication Centre (N2FC).

References

(1) Sang, L.; Liao, M.; Sumiya, M. A Comprehensive Review of Semiconductor Ultraviolet Photodetectors: from Thin Film to One-Dimensional Nanostructures. *Sensors (Basel)* **2013**, *13*, 10482-10518.

(2) Tsao, J. Y.; Chowdhury, S.; Hollis, M. A.; Jena, D.; Johnson, N. M.; Jones, K. A.; Kaplar, R. J.; Rajan, S.; Van de Walle, C. G.; Bellotti, E.; et al. Ultrawide-Bandgap Semiconductors: Research Opportunities and Challenges. *Adv. Electron. Mater.* **2018**, *4*, 1600501.

(3) Jabbar, H. D.; Fakhri, M. A.; Jalal AbdulRazzaq, M. Gallium Nitride-Based Photodiode: A review. *Materials Today: Proceedings* **2021**, *42*, 2829-2834.

(4) Raut, H. K.; Ganesh, V. A.; Nair, A. S.; Ramakrishna, S. Anti-Reflective Coatings: A Critical, in-Depth Review. *Energy Environ. Sci.* **2011**, *4*, 3779.

(5) Shanmugam, N.; Pugazhendhi, R.; Madurai Elavarasan, R.; Kasiviswanathan, P.; Das, N. Anti-Reflective Coating Materials: A Holistic Review from PV Perspective. *Energies* **2020**, *13*, 2631.

(6) Chiu, C. H.; Yu, P.; Kuo, H. C.; Chen, C. C.; Lu, T. C.; Wang, S. C.; Hsu, S. H.; Cheng, Y. J.; Chang, Y. C. Broadband and Omnidirectional Antireflection Employing Disordered GaN Nanopillars. *Opt. Express* **2008**, *16*, 8748-8754.

(7) Ko, Y. H.; Yu, J. S. Design and Fabrication of Antireflective GaN Subwavelength Grating Structures Using Periodic Silica Sphere Monolayer Array Patterning. *Appl. Phys. B* **2013**, *113*, 567-573.

(8) Chan, C. Y.; Namiki, S.; Hite, J. K.; Mastro, M. A.; Qadri, S. B.; Li, X. Homoepitaxial GaN Micropillar Array by Plasma-Free Photo-Enhanced Metal-Assisted Chemical Etching. *J. Vac. Sci. Technol., A* **2021**, *39*, 053212.

(9) Kim, H. J.; Park, J.; Ye, B. U.; Yoo, C. J.; Lee, J. L.; Ryu, S. W.; Lee, H.; Choi, K. J.; Baik, J. M. Parallel Aligned Mesopore Arrays in Pyramidal-Shaped Gallium Nitride and Their Photocatalytic Applications. *ACS Appl. Mater. Interfaces* **2016**, *8*, 18201-18207.
(10) Han, L.; Zhao, H. Surface Antireflection Properties of GaN Nanostructures with Various Effective Refractive Index Profiles. *Opt. Express* **2014**, *22*, 31907-31916.
(11) Han, L.; French, R. H.; Zhao, H. Surface Antireflection and Light Extraction Properties of GaN Microdomes. *IEEE Photonics Journal* **2015**, *7*, 1-9.
(12) Ramizy, A.; Hassan, Z.; Omar, K. Porous GaN on Si(111) and Its Application to Hydrogen Gas Sensor. *Sens. Actuators, B* **2011**, *155*, 699-708.
(13) Al-Heuseen, K.; Hashim, M. R. Enhancing Responsivity of Porous GaN Metal-Semiconductor-Metal Ultraviolet Photodiodes by Using Photoelectrochemical Etching. *Acta Phys. Pol., A* **2012**, *121*, 71-73.
(14) Choi, E. S.; Song, Y. M.; Park, G. C.; Lee, Y. T. Disordered Antireflective Subwavelength Structures Using Ag Nanoparticles for GaN-Based Optical Device Applications. *J. Nanosci. Nanotechnol.* **2011**, *11*, 1342-1345.
(15) Debnath, R.; Ha, J.-Y.; Wen, B.; Paramanik, D.; Motayed, A.; King, M. R.; Davydov, A. V. Top-Down Fabrication of Large-Area GaN Micro- and Nanopillars. *J. Vac. Sci. Technol., B* **2014**, *32*, 021204.
(16) Yang, C.; Xi, X.; Yu, Z.; Cao, H.; Li, J.; Lin, S.; Ma, Z.; Zhao, L. Light Modulation and Water Splitting Enhancement Using a Composite Porous GaN Structure. *ACS Appl. Mater. Interfaces* **2018**, *10*, 5492-5497.
(17) Lee, J.-M.; Chang, K.-M.; Kim, S.-W.; Huh, C.; Lee, I.-H.; Park, S.-J. Dry Etch Damage in n-Type GaN and Its Recovery by Treatment with An N_2 Plasma. *J. Appl. Phys.* **2000**, *87*, 7667-7670.
(18) Xu, K.; Xu, C.; Xie, Y.; Deng, J.; Zhu, Y.; Guo, W.; Xun, M.; Teo, K. B. K.; Chen, H.; Sun, J. Graphene GaN-Based Schottky Ultraviolet Detectors. *IEEE Trans. Electron Devices* **2015**, *62*, 2802-2808.
(19) Kodama, M.; Sugimoto, M.; Hayashi, E.; Soejima, N.; Ishiguro, O.; Kanechika, M.; Itoh, K.; Ueda, H.; Uesugi, T.; Kachi, T. GaN-Based Trench Gate Metal Oxide Semiconductor Field-Effect Transistor Fabricated with Novel Wet Etching. *Appl. Phys. Express* **2008**, *1*, 021104.
(20) Kawakami, R.; Inaoka, T. Effect of Argon Plasma Etching Damage on Electrical Characteristics of Gallium Nitride. *Vacuum* **2008**, *83*, 490-492.
(21) Lee, Y.-H.; Kang, J.-H.; Ryu, S.-W. Enhanced Photocurrent and Persistent Photoconductivity in Nanoporous GaN Formed by Electrochemical Etching. *Thin Solid Films* **2013**, *540*, 150-154.
(22) Park, J.; Kang, J.-H.; Ryu, S.-W. High Diffuse Reflectivity of Nanoporous GaN Distributed Bragg Reflector Formed by Electrochemical Etching. *Appl. Phys. Express* **2013**, *6*, 072201.
(23) Tian, Y.; Feng, P.; Zhu, C.; Chen, X.; Xu, C.; Esendag, V.; Martinez de Arriba, G.; Wang, T. Nearly Lattice-Matched GaN Distributed Bragg Reflectors with Enhanced Performance. *Materials (Basel)* **2022**, *15*, 3536.
(24) Zhao, D. G.; Jiang, D. S.; Zhu, J. J.; Liu, Z. S.; Zhang, S. M.; Liang, J. W.; Yang, H.; Li, X.; Li, X. Y.; Gong, H. M. Influence of Defects in n^--GaN Layer on The Responsivity of Schottky Barrier Ultraviolet photodetectors. *Appl. Phys. Lett.* **2007**, *90*, 062106.
(25) De-Gang, Z.; Shuang, Z.; Wen-Bao, L.; Xiao-Peng, H.; De-Sheng, J.; Jian-Jun, Z.; Zong-Shun, L.; Hui, W.; Shu-Ming, Z.; Hui, Y.; et al. Role of Ga Vacancies in Enhancing The Leakage Current of GaN Schottky Barrier Ultraviolet Photodetectors. *Chin. Phys. B* **2010**, *19*, 057802.
(26) Chin, V. W. L.; Tansley, T. L.; Osotchan, T. Electron Mobilities in Gallium, Indium, and Aluminum

Nitrides. *J. Appl. Phys.* **1994**, *75*, 7365-7372.
(27) Ainorkhilah, M.; Zainuriah, H.; Yushamdan, Y.; Yam, F. K.; Chuah, L. S.; Naser, M. A. Structural and Surface Studies of Undoped Porous GaN Grown on Sapphire. *Adv. Mater. Res.* **2012**, *620*, 45-49.
(28) Cheah, S. F.; Lee, S. C.; Ng, S. S.; Yam, F. K.; Abu Hassan, H.; Hassan, Z. Luminescence Evolution of Porous GaN Thin Films Prepared Via UV-Assisted Electrochemical Etching. *J. Lumin.* **2015**, *159*, 303-311.
(29) Díaz, D. J.; Williamson, T. L.; Adesida, I.; Bohn, P. W.; Molnar, R. J. Morphology and Luminescence of Porous GaN Generated via Pt-Assisted Electroless Etching. *J. Vac. Sci. Technol., B* **2002**, *20*, 2375.
(30) Guo, X. Y.; Williamson, T. L.; Bohn, P. W. Enhanced Ultraviolet Photoconductivity in Porous GaN Prepared by Metal-Assisted Electroless Etching. *Solid State Commun.* **2006**, *140*, 159-162.
(31) Bardwell, J. A.; Webb, J. B.; Tang, H.; Fraser, J.; Moisa, S. Ultraviolet Photoenhanced Wet Etching of GaN in $K_2S_2O_8$ Solution. *J. Appl. Phys* **2001**, *89*, 4142-4149.
(32) Perumal, R.; Hassan, Z. Nanoporous Gallium Nitride through Anisotropic Metal-Assisted Electroless Photochemical Wet Etching Technique. *Surf. Rev. Lett.* **2016**, *23*, 1550106.
(33) Wang, K. C.; Yuan, G. D.; Wu, R. W.; Lu, H. X.; Liu, Z. Q.; Wei, T. B.; Wang, J. X.; Li, J. M.; Zhang, W. J. GaN Nanowire Arrays by a Patterned Metal-Assisted Chemical Etching. *J. Cryst. Growth* **2016**, *440*, 96-101.
(34) Geng, X.; Duan, B. K.; Grismer, D. A.; Zhao, L.; Bohn, P. W. Catalyst and Processing Effects on Metal-Assisted Chemical Etching for the Production of Highly Porous GaN. *Semicond. Sci. Technol.* **2013**, *28*, 065001.
(35) Kim, S. H.; Mohseni, P. K.; Song, Y.; Ishihara, T.; Li, X. Inverse Metal-Assisted Chemical Etching Produces Smooth High Aspect Ratio InP Nanostructures. *Nano Lett.* **2015**, *15*, 641-648.
(36) Cowley, A.; Steele, J. A.; Byrne, D.; Vijayaraghavan, R. K.; McNally, P. J. Fabrication and Characterisation of GaAs Nanopillars Using Nanosphere Lithography and Metal Assisted Chemical Etching. *RSC Advances* **2016**, *6*, 30468-30473.
(37) Lee, J.-M.; Kim, B.-I. Thermal Dewetting of Pt Thin Film: Etch-Masks for the Fabrication of Semiconductor Nanostructures. *Mater. Sci. Eng.: A* **2007**, *449*, 769-773.
(38) Strobel, S.; Kirkendall, C.; Chang, J. B.; Berggren, K. K. Sub-10 nm Structures on Silicon by Thermal Dewetting of Platinum. *Nanotechnology* **2010**, *21*, 505301.
(39) Kawashima, T.; Yoshikawa, H.; Adachi, S.; Fuke, S.; Ohtsuka, K. Optical Properties of Hexagonal GaN. *J. Appl. Phys.* **1997**, *82*, 3528-3535.
(40) Huang, H. C.; Kim, M.; Zhan, X.; Chabak, K.; Kim, J. D.; Kvit, A.; Liu, D.; Ma, Z.; Zuo, J. M.; Li, X. High Aspect Ratio β-Ga_2O_3 Fin Arrays with Low-Interface Charge Density by Inverse Metal-Assisted Chemical Etching. *ACS Nano* **2019**, *13*, 8784-8792.
(41) Toguchi, M.; Miwa, K.; Horikiri, F.; Fukuhara, N.; Narita, Y.; Yoshida, T.; Sato, T. Electrodeless Photo-Assisted Electrochemical Etching of GaN Using a H_3PO_4-based Solution Containing $S_2O_8^{2-}$ Ions. *Appl. Phys. Express* **2019**, *12*, 031003.
(42) Horikiri, F.; Fukuhara, N.; Ohta, H.; Asai, N.; Narita, Y.; Yoshida, T.; Mishima, T.; Toguchi, M.; Miwa, K.; Ogami, H.; et al. Thermal-Assisted Contactless Photoelectrochemical Etching for GaN. *Appl. Phys. Express* **2020**, *13*, 046501.
(43) Kim, M.; Huang, H.-C.; Kim, J. D.; Chabak, K. D.; Kalapala, A. R. K.; Zhou, W.; Li, X. Nanoscale Groove Textured β-Ga_2O_3 by Room Temperature Inverse Metal-Assisted Chemical Etching and Photodiodes with Enhanced Responsivity. *Appl. Phys. Lett.* **2018**, *113*, 222104.
(44) Kim, M.; Yi, S.; Kim, J. D.; Yin, X.; Li, J.; Bong, J.; Liu, D.; Liu, S. C.; Kvit, A.; Zhou, W.; et al.

Enhanced Performance of Ge Photodiodes via Monolithic Antireflection Texturing and α-Ge Self-Passivation by Inverse Metal-Assisted Chemical Etching. *ACS Nano* **2018**, *12*, 6748-6755.
(45) Kunwar, S.; Pandey, P.; Sui, M.; Zhang, Q.; Li, M.-Y.; Lee, J. Nanoscale Morphology and Optical Property Evolution of Pt Nanostructures on GaN (0001) by the Systematic Control of Annealing Temperature and Duration with Various Pt Thickness. *Mater. Res. Express* **2017**, *4*, 065019.
(46) Li, D.; Sumiya, M.; Fuke, S.; Yang, D.; Que, D.; Suzuki, Y.; Fukuda, Y. Selective Etching of GaN Polar Surface in Potassium Hydroxide Solution Studied by X-Ray Photoelectron Spectroscopy. *J. Appl. Phys.* **2001**, *90*, 4219-4223.
(47) Reshchikov, M. A.; Morkoç, H. Luminescence Properties of Defects in GaN. *J. Appl. Phys.* **2005**, *97*, 5-19.
(48) Shalish, I.; Shapira, Y.; Burstein, L.; Salzman, J. Surface States and Surface Oxide in GaN Layers. *J. Appl. Phys.* **2001**, *89*, 390-395.
(49) Bergman, L.; Nemanich, R. J. Raman Spectroscopy for Characterization of Hard, Wide-Bandgap Semiconductors: Diamond, GaN, GaAlN, AlN, BN. *Annu. Rev. Mater. Sci.* **1996**, *26*, 551-579.
(50) Mohammed, F. K.; Beh, K. P.; Ramizy, A.; Ahmed, N. M.; Yam, F. K.; Hassan, Z. Improvement of Porous GaN-Based UV Photodetector with Graphene Cladding. *Appl. Sci.* **2021**, *11*, 10833.
(51) Van Der Pauw, L. J.; A Method of Measuring Specific Resistivity and Hall Effect of Discs of Arbitrary Shape. *Philips Res. Rep.* **1958**, *13*, 1-9.
(52) Lyons, J. L.; Wickramaratne, D.; Van de Walle, C. G. A First-Principles Understanding of Point Defects and Impurities in GaN. *J. Appl. Phys* **2021**, *129*, 111101.
(53) Takada, N.; Taoka, N.; Yamamoto, T.; Ohta, A.; Truyen, N. X.; Yamada, H.; Takahashi, T.; Ikeda, M.; Makihara, K.; Shimizu, M.; et al. Impact of Remote Plasma Oxidation of A GaN Surface on Photoluminescence Properties. *Jpn. J. Appl. Phys.* **2019**, *58*, SEEC02.
(54) Li, Z. F.; Lu, W.; Ye, H. J.; Chen, Z. H.; Yuan, X. Z.; Dou, H. F.; Shen, S. C.; Li, G.; Chua, S. J. Carrier Concentration and Mobility in Gan Epilayers on Sapphire Substrate Studied by Infrared Reflection Spectroscopy. *J. Appl. Phys.* **1999**, *86*, 2691-2695.
(55) Deinega, A.; Valuev, I.; Potapkin, B.; Lozovik, Y. Minimizing Light Reflection from Dielectric Textured Surfaces. *J. Opt. Soc. Am. A* **2011**, *28*, 770-777.
(56) Liao, Y.; Zheng, Y.; Shin, S. H.; Zhao, Z. J.; An, S.; Seo, J. H.; Jeong, J. H.; Kim, M. Distinct UV–Visible Responsivity Enhancement of GaAs Photodetectors via Monolithic Integration of Antireflective Nanopillar Structure and UV Absorbing IGZO Layer. *Adv. Opt. Mater.* **2022**, 2200062.
(57) Han, Q.; Fu, Y.; Jin, L.; Zhao, J.; Xu, Z.; Fang, F.; Gao, J.; Yu, W. Germanium Nanopyramid Arrays Showing near-100% Absorption in the Visible Regime. *Nano Research* **2015**, *8*, 2216-2222.
(58) Chen, Y. T.; Yang, C. Y.; Chen, P. C.; Sheu, J. K.; Lin, K. H. Carrier Dynamics of Mn-induced States in GaN Thin Films. *Sci. Rep.* **2017**, *7*, 5788.
(59) Cao, X. A.; Pearton, S. J.; Dang, G.; Zhang, A. P.; Ren, F.; Van Hove, J. M. Effects of Interfacial Oxides on Schottky Barrier Contacts to N- and P-Type GaN. *Appl. Phys. Lett.* **1999**, *75*, 4130-4132.
(60) Zhang, Y. Y.; Zheng, Y. X.; Lai, J. Y.; Seo, J. H.; Lee, K. H.; Tan, C. S.; An, S.; Shin, S. H.; Son, B.; Kim, M. High Performance Flexible Visible-Blind Ultraviolet Photodetectors with Two-Dimensional Electron Gas Based on Unconventional Release Strategy. *ACS Nano* **2021**, *15*, 8386.
(61) Rathkanthiwar, S.; Kalra, A.; Solanke, S. V.; Mohta, N.; Muralidharan, R.; Raghavan, S.; Nath, D. N. Gain Mechanism and Carrier Transport in High Responsivity AlGaN-Based Solar Blind Metal Semiconductor Metal Photodetectors. *J. Appl. Phys.* **2017**, *121*, 164502.
(62) Aggarwal, N.; Gupta, G. Enlightening Gallium Nitride-Based UV Photodetectors. *J. Mater. Chem.*

C **2020**, *8*, 12348-12354.
(63) Ramesh, C.; Tyagi, P.; Bhattacharyya, B.; Husale, S.; Maurya, K. K.; Kumar, M. S.; Kushvaha, S. S. Laser Molecular Beam Epitaxy Growth of Porous GaN Nanocolumn and Nanowall Network on Sapphire (0001) for High Responsivity Ultraviolet Photodetectors. *J. Alloys Compd.* **2019**, *770*, 572-581.
(64) Guo, Y.; Song, W.; Liu, Q.; Sun, Y.; Chen, Z.; He, X.; Zeng, Q.; Luo, X.; Zhang, R.; Li, S. A Porous GaN/MoO_3 Heterojunction for Filter-Free, Ultra-Narrowband Ultraviolet Photodetection. *J. Mater. Chem. C* **2022**, *10*, 5116-5123.
(65) Jiang, K.; Sun, X.; Chen, Y.; Zhang, S.; Ben, J.; Chen, Y.; Zhang, Z.-H.; Jia, Y.; Shi, Z.; Li, D. Three-Dimensional Metal–Semiconductor–Metal Bipolar Ultraviolet Phototransistor Based on GaN p-i-n Epilayer. *Appl. Phys. Lett.* **2021**, *119*, 161105.
(66) Tian, H.; Liu, Q.; Zhou, C.; Zhan, X.; He, X.; Hu, A.; Guo, X. Hybrid Graphene/Unintentionally Doped Gan Ultraviolet Photodetector with High Responsivity and Speed. *Appl. Phys. Lett.* **2018**, *113*, 121109.
(67) Zhang, X.; Li, J.; Ma, Z.; Zhang, J.; Leng, B.; Liu, B. Design and Integration of a Layered MoS_2/GaN van der Waals Heterostructure for Wide Spectral Detection and Enhanced Photoresponse. *ACS Appl. Mater. Interfaces* **2020**, *12*, 47721-47728.
(68) Tak, B. R.; Gupta, V.; Kapoor, A. K.; Chu, Y.-H.; Singh, R. Wearable Gallium Oxide Solar-Blind Photodetectors on Muscovite Mica Having Ultrahigh Photoresponsivity and Detectivity with Added High-Temperature Functionalities. *ACS Appl. Electron. Mater.* **2019**, *1*, 2463-2470.
(69) Garg, M.; Tak, B. R.; Rao, V. R.; Singh, R. Giant UV Photoresponse of GaN-Based Photodetectors by Surface Modification Using Phenol-Functionalized Porphyrin Organic Molecules. *ACS Appl. Mater. Interfaces* **2019**, *11*, 12017-12026.
(70) Lin, Z.-H.; Cheng, G.; Yang, Y.; Zhou, Y. S.; Lee, S.; Wang, Z. L. Triboelectric Nanogenerator as An Active UV Photodetector. *Adv. Funct. Mater.* **2014**, *24*, 2810-2816.